Received: 21 May 2018 | Accepted: 20 August 2018

DOI: 10.1002/jcb.27671

RESEARCH ARTICLE

WILEY Journal of Cellular Biochemistry

MAPKs and NF-κB-mediated acrylamide-induced neuropathy in rat striatum and human neuroblastoma cells SY5Y

Dandan Yan[1] | Xiaoqi Pan[2] | Jianling Yao[1] | Dun Wang[3] | Xu Wu[1] | Xiaoyi Chen[4] | Nian Shi[1] | Hong Yan[1]

[1]Department of Health Toxicology, MOE Key Lab of Environment and Health, School of Public Health, Tongji Medical College, Huazhong University of Science and Technology, Wuhan, China

[2]Department of Preventive Medicine, School of Public Health, Chengdu University of Traditional Chinese Medicine, Chengdu, China

[3]Department of Community Health Service Management Center, The Third Affiliated Hospital of Shenzhen University, Shenzhen, China

[4]Department of Nutrition and Food Hygiene, School of Public Health, Guangzhou Medical University, Guangzhou, China

Correspondence
Hong Yan, Department of Health Toxicology, MOE Key Lab of Environment and Health, School of Public Health, Tongji Medical College, Huazhong University of Science and Technology, 13 Hangkong-Road, Wuhan 430030, China.
Email: yanhong@mails.tjmu.edu.cn

Funding information
National Natural Science Foundation of China, Grant/Award Number: 81373042

Abstract

Acrylamide (ACR) is a potent neurotoxin that can be produced during high-temperature food processing, but the underlying toxicological mechanism remains unclear. In this study, the detrimental effects of ACR on the striatal dopaminergic neurons and the roles of mitogen-activated protein kinases (MAPKs) and nuclear factor κB (NF-κB) in ACR-induced neuronal apoptosis were investigated. Acute ACR exposure caused dopaminergic neurons loss and apoptosis as revealed by decreased tyrosine hydroxylase (TH)-positive cells and TH protein level and increased terminal deoxynucleotidyl transferase dUTP nick-end labeling (TUNEL)-positive cells in the striatum. ACR-decreased glutathione content, increased levels of malondialdehyde, proinflammatory cytokines tumor necrosis factor α, and interleukin 6. In addition, nuclear NF-κB and MAPKs signaling pathway with c-Jun N-terminal kinase (JNK) and p38 were activated by ACR. Specific inhibitors were used to explore the roles of MAPKs and NF-κB pathways in ACR-induced apoptosis in SH-SY5Y cells. Pretreatment with JNK-specific inhibitors SP600125 markedly upregulated the reduced B-cell lymphoma 2 (Bcl-2) content and downregulated the increased Bcl-2-associated X protein (Bax) level and thereby eventually reduced the proportions of early and late apoptotic cells induced by ACR, while p38 suppression by SB202190 only reversed the decrease in Bcl-2 expression. Inhibition of NF-κB by BAY 11-7082 markedly upregulated Bax level and decreased Bcl-2 expression, and eventually increasing the proportions of neuronal apoptosis compared with that in ACR alone. These results suggested that JNK contributed to ACR-induced apoptosis, while NF-κB acted as a protective regulator in response to ACR-induced neuropathy. This study helps to offer a deeper insight into the mechanism of ACR-induced neuropathy.

KEYWORDS

acrylamide, apoptosis, inflammation, mitogen-activated protein kinases, nuclear factor kappa B

Dandan Yan and Xiaoqi Pan contributed equally to this work.

1 | INTRODUCTION

Acrylamide (ACR) is a water-soluble vinyl monomer used in many applications in laboratories and chemical industry. In 2002, the Swedish National Food Administration first reported ACR is a by-product of the high-temperature cooking process, which is produced through Maillard reaction between reducing sugars and amino acids.[1,2] The discovery of ACR in the daily diet renewed the interests in its potential health effects and raised considerable concern. The International Agency for Research on Cancer and the US Environmental Protection Agency (1994) confirmed that ACR is a probable human carcinogen that elicits genotoxic, neurotoxic, and carcinogenic effects in several animal species[3]; however, only the neurotoxic effects are observed in humans. The neurotoxicity of ACR is characterized by ataxia, hindfoot splay, and hind limb muscle weakness.[4,5] The underlying mechanism has been considered to be associated with nerve terminals[6] and axonal damage, which is classified as central-peripheral distal axonopathy.[4] Dopamine, a well-known neurotransmitter, plays an important role in the central nervous system in regulating some vital physiological and pathological functions, including motor, cognition, and neuroendocrine activity.[7] Striatum contains a large number of dopaminergic neurons and it is identified as the largest integrated processing element in the basal ganglia.[8] Our current study is focused on the detrimental effects of ACR on the striatal dopaminergic neurons.

Intracerebroventricular instillations of selective toxicants are frequently applied to the lateral ventricles of laboratory animals for experimental purposes. It allows high concentrations of selective toxicants to enter the central compartment because it bypasses the brain barrier and other mechanisms that limit distribution of the administered substance into the brain.[9] ACR can impair blood-cerebrospinal fluid barrier and enter the central nervous system, but the dose is very low.[10] Furthermore, the majority of ACR when administered by oral or intraperitoneal injection is metabolized to glycidamide (GA) by cytochrome P450-2E1 in the hepatic microsomes. GA reacts with DNA to form DNA adducts and is responsible for the carcinogenicity and genotoxicity of ACR.[11,12] While the neurotoxicity of ACR is mainly associated with the ACR monomer itself.[13] Thus, in our present in vivo study the intracerebroventricular injection was used to directly transmit ACR to the neurons and avoid the formation of GA. Morphologies of neurons, loss of dopaminergic neurons and neuronal apoptosis, redox status and inflammation response are used to evaluate the neuropathy of ACR in this model.

Our previous research proposed that ACR led to oxidative stress in rat cerebellum.[14] Oxidative stress is known to activate nuclear factor κB (NF-κB) signaling and its controlled cytokine release such as tumor necrosis factor α (TNF-α) and interleukin 6 (IL-6).[15] Inflammation of the central nervous system is a prominent feature in many neurodegenerative diseases. Apoptosis is modulated by complex pathways that are involved in a series of biochemical regulators and molecular interactions. NF-κB is a ubiquitous transcription factor, and has been widely investigated because of its role as an inducible regulator of inflammation, cell survival, transformation, and apoptosis.[16,17] In the nervous system, NF-κB plays a dual role in neurodegenerative diseases; NF-κB activation in neurons promotes neuronal survival, while its activation in glial and immune cells mediates pathological inflammatory processes.[18] Mitogen-activated protein kinases (MAPKs) are serine/threonine protein kinases, and can be activated by cellular stresses. The MAPKs and NF-κB pathways regulate the expression of apoptosis-related proteins, and have positive and/or negative effects on apoptosis, depending on the cell types and the nature of stimulus. The roles of MAPKs and NF-κB signaling pathways in ACR-induced neurotoxicity are still unclear and need further study.

This study aims to investigate the detrimental effects of acute exposure to ACR through intracerebroventricular injection on striatal neurons, and to explore the roles of MAPKs and NF-κB signaling pathways in ACR-induced apoptosis in SH-SY5Y cells. This study helps to offer a deeper insight into the mechanism of ACR-induced neuropathy.

2 | MATERIALS AND METHODS

2.1 | Animal experimental protocol and tissue preparation

Twenty-eight male Sprague-Dawley rats (200 to 220 g, SPF class; provided by the Animal Experimental Center of Tongji Medical College, Huazhong University of Science and Technology) were fed freely with food and water for 1 week of acclimatization and then randomly assigned to four groups (control, 0.5 mg/kg ACR, 2.5 mg/kg ACR, and 12.5 mg/kg ACR) according to their body weight. The rats in the treatment groups were administered with ACR via the intracerebroventricular injection, and the rats in the control group were treated with isovolumetric artificial cerebral spinal fluid (ACSF) via the intracerebroventricular injection. Twenty-four hours later, the rats were killed and their brains were collected in accordance with the surgical protocol described in our instruction manual. The experiments were carried out according to the current regulations of the Institutional Animal Ethics Committee, and were approved by the Tongji Medical College Council on Animal Care

Committee, Huazhong University of Science and Technology (China).

Briefly, the rats were anesthetized by intraperitoneally injection of 2% sodium pentobarbital (30 mg/kg body weight), the skull was exposed, and a pair of symmetric holes was drilled (0.8 mm posterior to bregma, ±1.5 mm lateral, 3.4 mm dorsoventral) in a stereotaxic frame (RWD Life Science Co. Ltd., Shenzhen, China). A mini osmotic pump (RWD Life Science Co. Ltd) containing ACSF (10 μL) or ACR solution was slowly implanted into one of the symmetric holes of the rats within 5 minutes. After 5 minutes, the other side was also implanted with either ACSF or ACR solution to balance the concentration in the two sides of the ventricle. The wound was subsequently disinfected and sutured, and the rats were intraperitoneally injected with penicillin to prevent infection.

Twenty-four hours after treatment, the rats were killed through decapitation under anesthesia. Their brains were removed immediately and separated sagittally in two hemispheres. The left hemisphere was fixed in 4% ice-cold buffered paraformaldehyde and embedded in paraffin. The striatum of the right hemisphere was dissected and frozen immediately in liquid nitrogen and stored at −80°C for protein extraction.

2.2 | Cell culture and treatment

Human neuroblastoma SH-SY5Y cells were maintained at 37°C with 5% CO_2 in a 1:1 mix of Dulbecco modified Eagle medium and F-12K medium supplemented with 10% heat-inactivated fetal bovine serum with 0.1% penicillin/streptomycin. The medium was changed every 2 days, and the stock cultures were separated into new culture bottles every 3 days. The medium was replaced with serum-free medium, and the cells were treated with different concentrations of ACR (0, 1.25, 2.5, and 5 mM). The cells were then seeded in a six-well plate to observe the effects of ACR on morphological alterations. After treatment with different concentrations of ACR for 24 hours, the cells were photographed under a phase contrast microscope (IX71; Olympus Corporation, Tokyo, Japan). Cell viability was indirectly evaluated by 3-(4,5-dimethylthiazol-2-yl)-2,5-diphenyltetrazolium bromide (MTT) assay. SH-SY5Y cells were seeded in a 96-well plate at a density of 1×10^4 cells per well. The medium was replaced with serum-free medium containing different concentrations of ACR (0 to 5 mM). After incubation for 24 hours, the cells were treated with MTT solution for 4 hours at 37°C. Then the solution was removed and the formazan crystals were dissolved in dimethyl sulfoxide solution. The absorbance at 490 nm was determined in a microplate reader.

2.3 | Nissl staining

For Nissl staining, the slices of the rat brain were hydrated in serial concentrations of ethanol and incubated in 0.1% cresyl violet solution for 30 minutes. The slides were briefly immersed in 95% ethanol to remove excess stain and then rinsed with double-distilled water. The brain slices were subsequently dehydrated, and the sections were cleared in two serial concentrations of xylene solution, mounted with Canada balsam, and observed under a light microscope (80ITRFL-4; Nikon, Tokyo, Japan).

2.4 | TUNEL staining

Terminal deoxynucleotidyl transferase dUTP nick-end labeling (TUNEL) staining was performed using a kit (ISCDD; Boehringer, Mannheim, Germany) in accordance with the manufacturer's instructions. Briefly, the sections were washed with 0.1M phosphate-buffered saline (PBS) (pH 7.4) for 30 minutes, incubated in blocking solution at room temperature for 10 minutes, washed with PBS for 5 minutes, treated with permeabilization solution in an ice bat for 2 minutes, and washed three times with PBS for 10 minutes each. The sections were then incubated in TUNEL reaction solution in a humidified chamber at 37°C for 1 hour, washed three times with PBS, and incubated further in an antifluorescein antibody conjugated with horse-radish peroxidase at 37°C for 30 minutes. Afterward, sections were washed and treated with 3,3′-diaminobenzidine (DAB; Roche Diagnostics, Mannheim, Germany) solution for 2 minutes, washed three times with PBS, dehydrated, and mounted. Images were captured and digitized under an inverted fluorescence microscope (IX71; Olympus).

2.5 | Immunohistochemistry

Tyrosine hydroxylase (TH)-positive cells were analyzed through immunohistochemistry staining under standard conditions. Consecutive 4-μm–thick coronal rat brain sections were cut, dewaxed, rehydrated, and successively treated with 0.3% Triton X-100 and 3% bovine serum albumin for 1 hour at room temperature. Then, each whole mount was incubated overnight with rabbit polyclonal primary antibody at 4°C and further developed with biotin-conjugated secondary antibody for 2 hours. Immunoreactivity was visualized with DAB and counterstained with hematoxylin. The sections were then mounted in a permanent mounting medium. Negative controls were obtained by omitting the primary antibodies. Three sections for each sample were evaluated, and the immune stained sections of the striatum was examined under a conventional microscope (Olympus BX51; Olympus Corporation) at ×400

magnification and recorded with a digital camera (Olympus DP70; Olympus Corporation).

2.6 | Measurement of lipid peroxidation and glutathione

The malondialdehyde (MDA) and glutathione (GSH) content of the striatum tissue and SH-SY5Y cells were detected through a colorimetric microplate assay. A spectrophotometric method was applied to determine GSH and MDA levels according to the manufacturer's instructions (Nanjing Jiancheng Bioengineering Institute, Nanjing, China). Protein concentrations were identified with Bradford method. MDA content and GSH level were expressed as nanomole per milligram protein.

2.7 | Measurement of reactive oxygen species level in SH-SY5Y cells

Intracellular reactive oxygen species (ROS) oxidative state was detected using the probe dichloro-dihydro-fluorescein diacetate (DCFH-DA). After preparation, the cells were collected and incubated with DCFH-DA solution (100 μmol/L) at 37°C for 30 minutes. After incubation with the fluorescence probe, the cells were washed with the buffer. DCF fluorescence was excited at 488 nm with an argon laser, and the evoked emission was filtered with a 525-nm long pass filter. Fluorescence intensity was determined with a microplate reader.

2.8 | Cytokine assessment

The contents of TNF-α and IL-6 in the striatum and SH-SY5Y cells were measured using rat enzyme-linked immunosorbent assay (ELISA) kits (Elabscience Biotechnology Co. Ltd, Wuhan, China). Frozen tissues or cells were homogenized and sonicated in ice-cold PBS containing protease inhibitors (Complete Protease Inhibitor Cocktail; Roche Diagnostics). Homogenates were centrifuged at 5000*g* for 8 minutes at 4°C, and the resultant supernatant was collected. The extracts were loaded onto ELISA plates induplicate in accordance with the manufacturer's instructions. TNF-α and IL-6 standards were prepared in a buffer with the same composition of final tissue samples.

2.9 | High-performance liquid chromatographic analysis of dopamine in SH-SY5Y cells

Contents of dopamine in SH-SY5Y cells was analyzed by high-performance liquid chromatographic (HPLC)-fluorescence detection. The mobile phase consisted of buffer saline (0.02M sodium citrate and 0.05M sodium hydrogen phosphate) and methanol (95:5 v/v), and the flow rate was maintained at 1.0 mL/min. The treated cells were homogenized in PBS, centrifuged at 40 000*g* for 10 minutes and injected volume was 20 μL. Standard curve and linear range were determined using dopamine standards. Dopamine level was calculated from the standard curve equation and reported as microgram of dopamine per gram of protein. The wavelength λEx = 285 nm, λEm = 333 nm.

2.10 | Quantification of apoptosis in SH-SY5Y cells

Cell apoptosis was analyzed by annexin V (AV)-fluorescein isothiocyanate (FITC)/propidium iodide (PI) apoptosis kit. In brief, SH-SY5Y cells were pretreated with c-Jun N-terminal kinase (JNK), p38, or NF-κB inhibitor (SP600125, SB202190, BAY 11-7082; MedchemExpress, Monmouth Junction, NJ) for 2 hours, and then incubated with 2.5 mM ACR for 24 hours. Total cells (2×10^5 cells per well) were collected and resuspended in 500 μL of binding buffer. Afterward, 5 μL of AV-FITC and 10 μL of PI were added to each sample and incubated at room temperature for 5 minutes away from light. The numbers of AV-negative/PI-positive, AV-positive/PI-positive, AV-positive/PI-negative, and unlabeled cells were determined through flow cytometry. AV-FITC binding was evaluated by a flow cytometer (Ex = 488 nm, Em = 530 nm) equipped with a FITC signal detector, and PI staining was assessed by a phycoerythrin emission signal detector. Data were analyzed using CellQuest Software (Media Cybernetics), and 10 000 events were analyzed for each independent.

2.11 | Western blot analysis

Total proteins from striatum and SH-SY5Y cells were isolated using a protein extraction kit (Bio-Rad, Hercules, CA) and then quantified with a BCA assay kit (Boster Biological Technology, Wuhan, China). Protein samples were denatured by mixing with sodium dodecyl sulfate (SDS) sample buffer and boiled at 98°C for 5 minutes. An aliquot containing 50 μg protein of the supernatant was loaded into SDS-PAGE gel (8% to 12%), separated electrophoretically, and transferred to a polyvinylidene fluoride (PVDF) membrane (Millipore, Bedford, MA). After the PVDF membrane was incubated with 5% bovine serum albumin to block nonspecific protein binding, the membranes were incubated overnight at 4°C with primary antibodies against extracellular signal–regulated kinase (ERK)1/2, JNK, p38, p-ERK, p-JNK, p-p38, NF-κB, nuclear transcription factor E2–related factor 2 (Nrf2), B-cell lymphoma 2 (Bcl-2), Bcl-2-associated X protein (Bax), and β-actin (Cell Signaling Technology, Danvers, MA) at 1:1000 dilutions. The blots

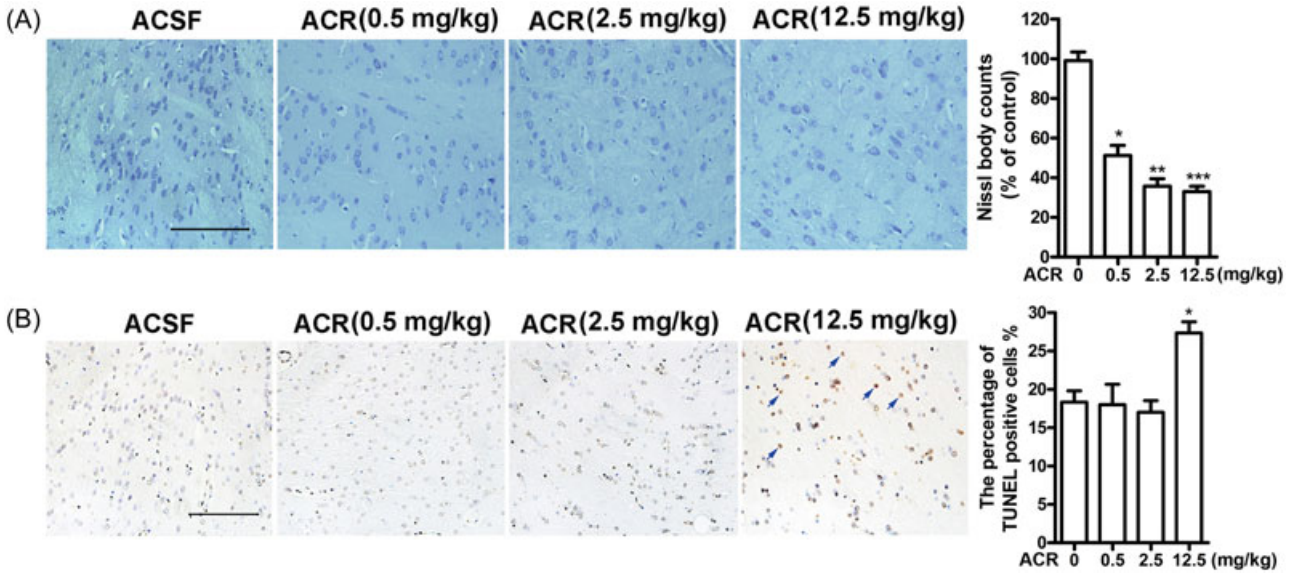

FIGURE 1 Acute exposure to ACR induced pathomorphological changes and apoptosis in rat striatum. Rats were administered with 0.5, 2.5, and 12.5 mg/kg ACR dissolved in ACSF solutions by intracerebroventricular injection. A, The striatal neurons were observed by Nissl staining (×200). Nissl body in randomly selected areas of digital images was counted using Image-Pro Plus 6.0 (Media Cybernetics). B, Apoptotic neurons in the striatum were observed by TUNEL staining (×200). TUNEL-positive cells in randomly selected areas of digital images was assayed using Image-Pro Plus 6.0. Arrows showed TUNEL-positive cells. Data were expressed as means ± SD ($n = 3$). *$P < 0.05$, **$P < 0.01$, ***$P < 0.001$ vs the solvent controls. ACR, acrylamide; ACSF, artificial cerebral spinal fluid; TUNEL, terminal deoxynucleotidyl transferase dUTP nick-end labeling

were then incubated with secondary antibodies (Cell Signaling Technology, Beverly, MA) at 1:3000 dilutions for 1.5 hours at room temperature. Protein expression was detected with an enhanced chemiluminescence method (Thermo Fisher Scientific, MA). Images were acquired and examined by the GeneSnap and GeneTools software (Syngene, Bio-Rad, Hercules, CA), respectively. Protein expression levels were normalized against internal standard intensity for data analysis.

2.12 | Statistical analysis

Data were analyzed in SPSS version 12.0 for Windows (SPSS Inc, Chicago, IL) and presented as mean ± SD. Statistical analyses were performed using one-way analysis of variance followed by Newman-Keuls post hoc test. All experiments were conducted independently at least three times. In all of the comparisons, statistical significance was obtained at $P < 0.05$.

3 | RESULTS

3.1 | Acute exposure to ACR induced pathomorphological changes and apoptosis in rat striatum

There were no obvious abnormal changes in weight gain, gait score, and other behavioral manifestations in the four groups. Nissl body is a characteristic structure in the somatic cytoplasm of neurons. Nissl staining was performed to determine the effects of ACR on the neurons in the rat striatum. The striatal neurons in 0.5, 2.5, and 12.5 mg/kg ACR groups contained pyknotic nuclei, exhibited a disappearance of Nissl substance, appeared swollen, and showed an irregular arrangement. Moreover, the number of Nissl body in 0.5, 2.5, and 12.5 mg/kg ACR groups was significantly diminished relative to the control value (Figure 1A; $P < 0.5$).

Apoptotic neuronal death was evaluated by TUNEL staining. The TUNEL-positive cells were rarely detected in the striatum of control, 0.5 mg/kg, and 2.5 mg/kg ACR groups. Conversely, the number of TUNEL-positive cells in the rats injected with 12.5 mg/kg ACR was significantly increased (Figure 1B; $P < 0.05$). These results indicated that acute exposure to ACR caused neuronal apoptosis in the striatum.

3.2 | Acute exposure to ACR induced loss of dopaminergic neurons in rat striatum

TH is the key enzyme for dopamine synthesis, and TH-positive cells represents dopaminergic neurons. To explore the effects of ACR on dopaminergic neurons in rat striatum, TH protein expression and TH-positive cells were examined by Western blot analysis and

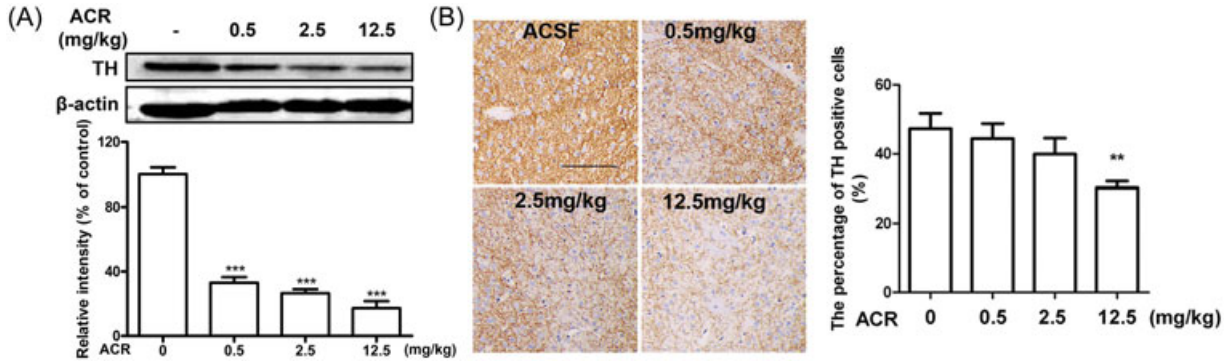

FIGURE 2 Acute exposure to ACR induced loss of dopaminergic neurons in rat striatum. Rats were administered with 0.5, 2.5, and 12.5 mg/kg ACR dissolved in ACSF solutions by intracerebroventricular injection. A, Western blot analysis was performed to assess TH protein expression. Results were expressed as relative intensity with β-actin as the internal control in striatum. B, TH-positive cells were detected by immunohistochemistry and then observed with a microscope (×200). TH-positive expression in randomly selected areas of digital images was assayed using Image-Pro Plus 6.0. Data are expressed as mean ± SD ($n = 3$). *$P < 0.05$, **$P < 0.01$, ***$P < 0.001$ vs the solvent controls. ACR, acrylamide; ACSF, artificial cerebral spinal fluid; TH, tyrosine hydroxylase

immunohistochemistry. The Western blot analysis demonstrated that the TH protein expression in 0.5, 2.5, and 12.5 mg/kg ACR groups remarkably decreased compared with that in the control group (Figure 2A; $P < 0.001$). Moreover, immunohistochemistry showed that the number of TH-positive cells decreased significantly in the rats injected with 12.5 mg/kg ACR (Figure 2B; $P < 0.01$). This finding indicated significant loss of striatal dopaminergic neurons after ACR treatment by intracerebroventricular injection.

3.3 | Acute exposure to ACR increased oxidative stress in the striatum

Figure 3A showed MDA level in the striatum was apparently increased after the rats administered with 2.5 and 12.5 mg/kg ACR. The amount of GSH, an essential antioxidant, was markedly decreased in 0.5, 2.5, and 12.5 mg/kg ACR groups (Figure 3B; $P < 0.01$). The Nrf2 plays an important role in protection against oxidative damage by binding to antioxidant response elements.[19] Western blot analysis showed the protein level of striatal nuclear Nrf2 in ACR exposure groups remained unchanged relative to that in the control group (Figure 3C). Collectively, these results indicated exposure to ACR by acute intracerebroventricular injection resulted in oxidative stress in rat striatum.

3.4 | Acute exposure to ACR increased the protein level of nuclear NF-κB and the resultant release of proinflammatory cytokines in rat striatum

The striatum was collected for ELISA to determine the contents of TNF-α and IL-6. The results revealed that

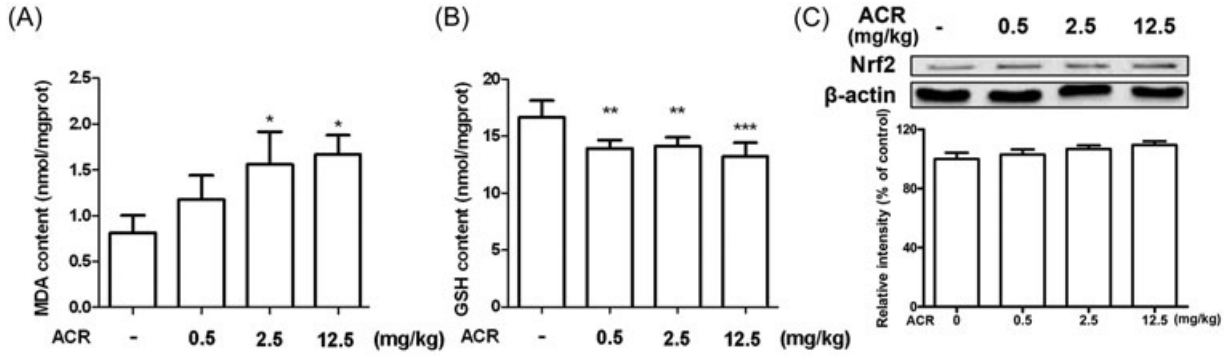

FIGURE 3 Acute exposure to ACR increased oxidative stress in the striatum. Rats were administered with 0.5, 2.5, and 12.5 mg/kg ACR dissolved in ACSF solutions by intracerebroventricular injection. A, MDA generation and (B) GSH content were detected. C, Nuclear Nrf2 expression was determined by Western blot analysis. The results were expressed as fold increases of optical density with β-actin serving as internal control. Data are expressed as mean ± SD ($n = 6$). *$P < 0.05$, **$P < 0.01$, ***$P < 0.001$ vs the solvent controls. ACR, acrylamide; ACSF, artificial cerebral spinal fluid; GSH, glutathione; MDA, malondialdehyde; Nrf2, nuclear transcription factor E2–related factor 2

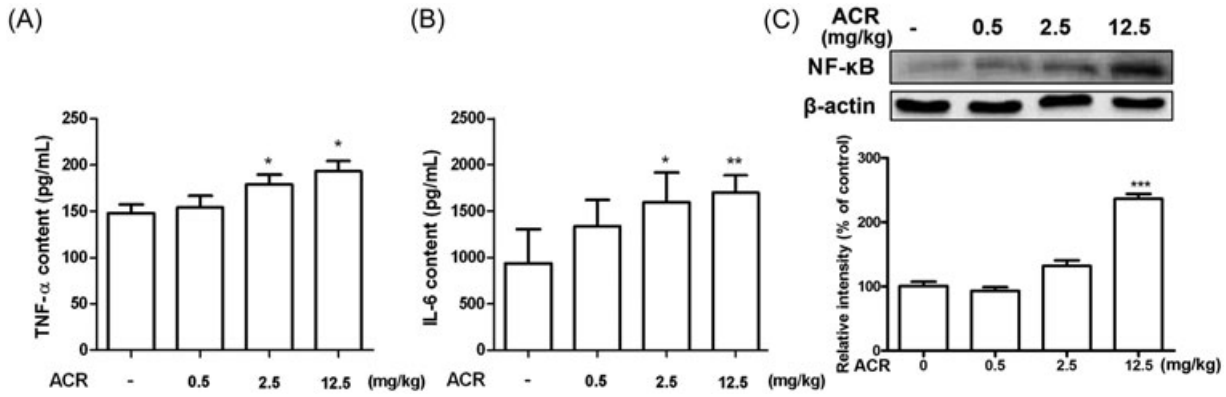

FIGURE 4 Acute exposure to ACR increased the protein level of nuclear NF-κB and the resultant release of proinflammatory cytokines in rat striatum. Rats were administered with 0.5, 2.5, and 12.5 mg/kg ACR dissolved in ACSF solutions by intracerebroventricular injection. (A) TNF-α level and (B) IL-6 content were determined by ELISA. C, Nuclear NF-κB expression was determined by Western blot analysis. The results were expressed as fold increases of optical density with β-actin serving as internal control. Data are expressed as mean ± SD ($n = 6$). *$P < 0.05$, **$P < 0.01$, ***$P < 0.001$ vs the solvent controls. ACR, acrylamide; ACSF, artificial cerebral spinal fluid; ELISA, enzyme-linked immunosorbent assay; ERK, extracellular signal–regulated kinase; IL-6, interleukin 6; JNK, c-Jun N-terminal kinase; NF-κB, nuclear factor κB; TNF-α, tumor necrosis factor α

TNF-α and IL-6 contents in the groups injected with 2.5 and 12.5 mg/kg ACR were higher than those in the control group (Figures 4A and 4B). The NF-κB signal pathway is associated with regulating inflammation response. We next examined the level of nuclear NF-κB in the rat striatum through Western blot analysis. As shown in Figure 4C, nuclear NF-κB was considerably enhanced to 2.38-fold in rat striatum after the rats were injected with 12.5 mg/kg ACR when compared with that in control group. These results indicated that acute exposure to ACR by intracerebroventricular injection increased the level of nuclear NF-κB and induced inflammation in the present animal model.

3.5 | Acute exposure to ACR activated the MAPKs in the striatum

MAPK pathways comprises ERK1/2, JNK, and p38 signaling, which contribute to the pathology of various neurodegenerative disorders. To determine the involvement of various MAPK signaling pathways in ACR-induced neuropathy, we investigated the levels of p-ERK, p-JNK, and p-p38 through Western blot analysis. As shown in Figure 5, the p-JNK level was significantly increased in rats injected with 12.5 mg/kg ACR, and p-p38 level was markedly enhanced in the rats treated with 2.5 and 12.5 mg/kg ACR. The levels of p-ERK

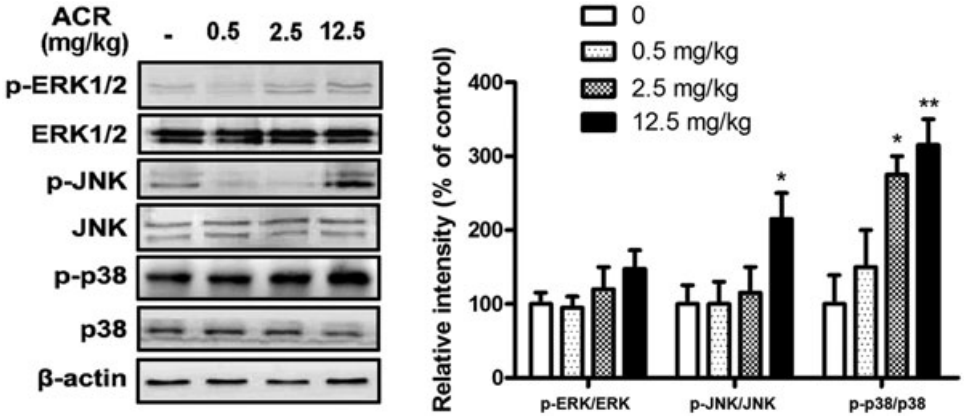

FIGURE 5 Acute exposure to ACR activated the MAPKs in the striatum. Protein expression of p-ERK1/2, total ERK1/2, p-JNK, total JNK, p-p38, and total p38 in striatum were determined by Western blot analysis. The results were expressed as fold increases of optical density with β-actin serving as internal control. Data are expressed as mean ± SD ($n = 6$). *$P < 0.05$, **$P < 0.01$, ***$P < 0.001$ vs the solvent controls. ACR, acrylamide; ERK, extracellular signal–regulated kinase; JNK, c-Jun N-terminal kinase; MAPK, mitogen-activated protein kinase

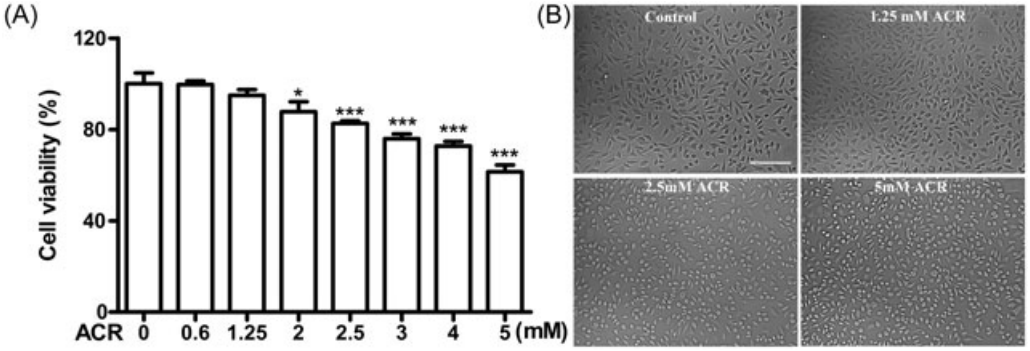

FIGURE 6 ACR-induced cytotoxicity in SH-SY5Y cells. A, Cell viability was determined by MTT assay as previously described in cells treated with 0 to 5 mM ACR for 24 hours. B, The morphology of cells treated with 0, 1.25, 2.5, and 5 mM ACR for 24 hours was observed under a microscope, scale bar = 100 μm. Data are expressed as mean ± SD ($n = 6$). *$P < 0.05$, **$P < 0.01$, ***$P < 0.001$ vs the vehicle control group. ACR, acrylamide; MTT, 3-(4,5-dimethylthiazol-2-yl)-2,5-diphenyltetrazolium bromide

and total JNK, ERK, and p38 remained unchanged in the four groups.

3.6 | Cytotoxicity of ACR on SH-SY5Y cells

SH-SY5Y cells were incubated with different concentrations of ACR for 24 hours and cell viability was assessed by MTT assay. As shown in Figure 6A, cell viability was significantly reduced in cells treated with 2 to 5 mM ACR in a dose-dependent manner. Figure 6B displayed the morphological changes of cells. Untreated SH-SY5Y cells were long and fusiform in shape with slender processes. After exposure to 2.5 or 5 mM of ACR for 24 hours, most cells shrank and the cell body became round.

3.7 | Effects of ACR on oxidative stress, proinflammatory cytokines, and dopamine level in SH-SY5Y cells

The redox status in SH-SY5Y cells was determined by the contents of the intracellular GSH, MDA, and ROS. The results illustrated treatment with 2.5 and 5 mM ACR dose dependently decreased intracellular GSH production (Figure 7A; $P < 0.001$) and increased MDA and ROS generation (Figures 7B and 7C; $P < 0.05$). The intracellular TNF-α and IL-6 contents in SH-SY5Y cells were measured to investigate the proinflammatory effects of ACR. The results demonstrated that TNF-α content was markedly boosted after treatment with 2.5 and 5 mM ACR relative to the control value (Figure 7D; $P < 0.001$); while IL-6 level was significantly increased only in 5 mM ACR as compared with that in the control group (Figure 7E; $P < 0.001$). Similar to the results of in vivo study, these data suggested that ACR caused intracellular oxidative stress and inflammation in SH-SY5Y cells.

Dopamine level in SH-SY5Y cells was analyzed by HPLC. As shown in Figure 7F, the iterative experiments produced a corresponding marked reduction in dopamine levels after treatment with ACR. In the presence of 1.25, 2.5, and 5 mM ACR, dopamine levels decreased to 76.3% ($P < 0.05$), 67.1% ($P < 0.01$), and 57.9% ($P < 0.001$) of the control value, respectively.

3.8 | Regulatory effects of JNK, p38, and NF-κB on ACR-induced apoptosis in SH-SY5Y cells

The specific inhibitors were used to investigate the regulatory effects of JNK, p38, and NF-κB on ACR-induced apoptosis in SH-SY5Y cells. Cells were pretreated with 20 μM SP600125 (JNK inhibitor), 10 μM SB202190 (p38 inhibitor), or 2 μM BAY 11-7082 (NF-κB inhibitor) for 2 hours and then incubated with 2.5 mM ACR for 24 hours. The apoptotic protein expression and the proportions of apoptotic cells were detected by Western blot analysis and flow cytometry, respectively. As shown in Figure 8A, compared with the ACR-treated group, cells pretreated with SP600125 showed a decreased proapoptotic Bax expression and increased antiapoptotic Bcl-2 formation when JNK pathway was blocked. Inhibition of p38 by SB202190 significantly enhanced Bcl-2 expression, but had no significant effect on Bax expression (Figure 8B). Pretreatment with BAY 11-7082 to inhibit NF-κB markedly enhanced Bax and decreased Bcl-2 expression compared with the ACR-treated group (Figure 8C). Accordingly, inhibition of JNK by SP600125 reduced the early and late apoptotic cells, pretreatment with BAY 11-7082 to inhibit NF-κB resulted in marked enhancement of the early apoptosis; however, the proportion of apoptotic cells remained unchanged when p38 was repressed by SB202190 (Figure 8D).

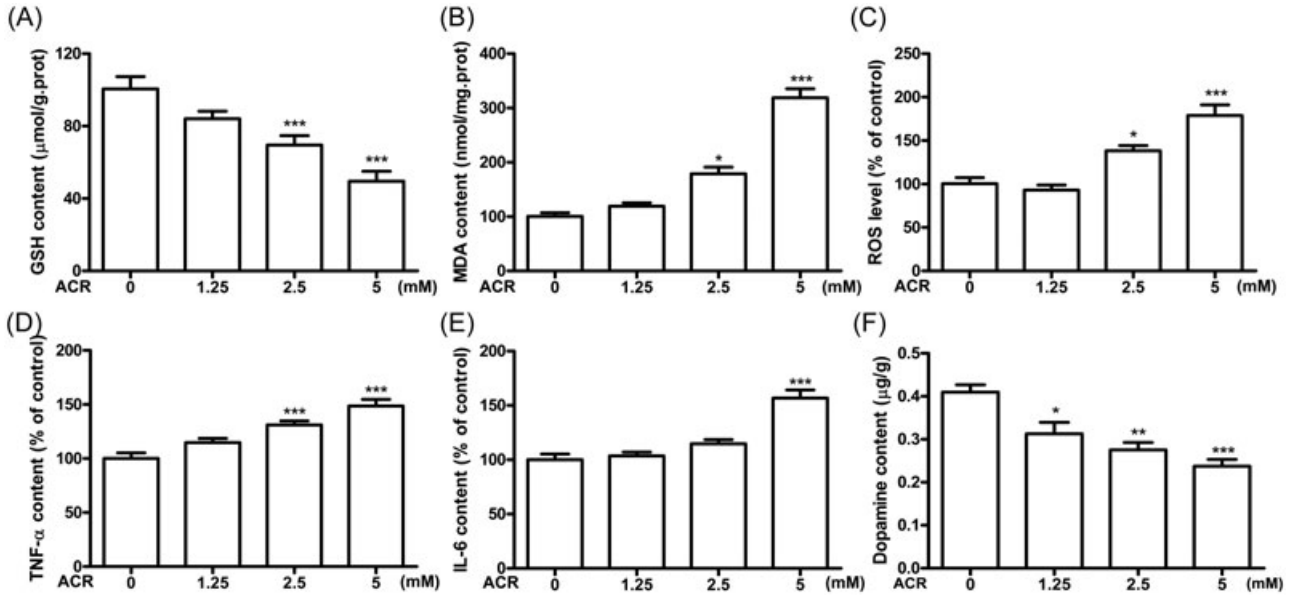

FIGURE 7 ACR-induced oxidative stress, proinflammatory cytokines, and dopamine level decline in SH-SY5Y cells. Cells were stimulated with ACR (1.25, 2.5, and 5 mM) for 24 hours. A, Antioxidant GSH level, (B) lipid peroxidant MDA content, (C) intracellular ROS were quantified. D, The TNF-α level and (E) IL-6 content in cells were determined. (F) The intracellular dopamine level was detected by HPLC. Data are expressed as mean ± SD ($n = 6$). *$P < 0.05$, **$P < 0.01$, ***$P < 0.001$ vs the vehicle control group. ACR, acrylamide; GSH, glutathione; HPLC, high-performance liquid chromatographic; IL-6, interleukin 6; MDA, malondialdehyde; ROS, reactive oxygen species; TNF-α, tumor necrosis factor α

4 | DISCUSSION

In this study, we investigated the adverse effects of acute exposure to ACR by intracerebroventricular injection on the neurons in rat striatum and especially the regulatory mechanism of nuclear NF-κB and MAPKs signaling pathways in ACR-induced apoptosis.

Over the past decades, the neurotoxicity of ACR has been extensively studied in animals. The majority of traditional exposure models of ACR were carried out by oral or intraperitoneal injection and the exposure time ranged from days to months. Although those models are more similar to the natural humans' intake ways, the comprehensive signs and symptoms of animals are often accompanied by significant weight loss or even death of animals, which may interfere the mechanism exploration. Furthermore, in traditional exposure models, ACR was metabolized in liver into GA which can react with DNA to form DNA adducts. This GA-DNA adducts are mainly responsible for the carcinogenicity and genotoxicity, while the neurotoxicity of ACR is mainly associated with the ACR monomer itself. To avoid the comprehensive toxicity of ACR and the disturbance of GA formation, our current study was conducted by treating rats with intracerebroventricular injection of ACR. The result showed 24 hours after ACR treatment, while no additional poisoning or symptoms were observed in rats, the changes of neuronal morphologies, the number of TH-positive and TUNEL-positive cells, cells' redox status and inflammation response were consistent with that in traditional models, indicating the intracerebroventricular injection is a suitable model to investigate the mechanisms of ACR neurotoxicity.

TH is a rate-limiting enzyme responsible for dopamine synthesis. TH protein expression and the TH-positive cells were assayed by Western blot analysis and immunocytochemistry. These results demonstrated a significant decreased TH protein expression and loss of dopaminergic neurons in the striatum of ACR-treated rats. Moreover, in vitro study found 1.25, 2.5, and 5 mM ACR declined the dopamine level in SH-SY5Y cells. These results agree well with other studies, which indicated that the dopaminergic neuron is one of primary sites of ACR action.[20-22] TUNEL staining was conducted to investigate whether the neuron loss is due to apoptosis. The result showed that high dose of ACR markedly increased the TUNEL-positive cells in rat striatum. Parkinson disease (PD) is a chronic neurodegenerative disease, which is characterized by a selective loss of dopaminergic neurons in the substantia nigra and striatum. The current work found ACR-induced degeneration and apoptosis of striatal dopaminergic neurons, suggesting that ACR may be one of the environmental risk factors of PD.

Oxidative stress is linked to the development of neuronal dysfunction and neuron death.[15] Previous

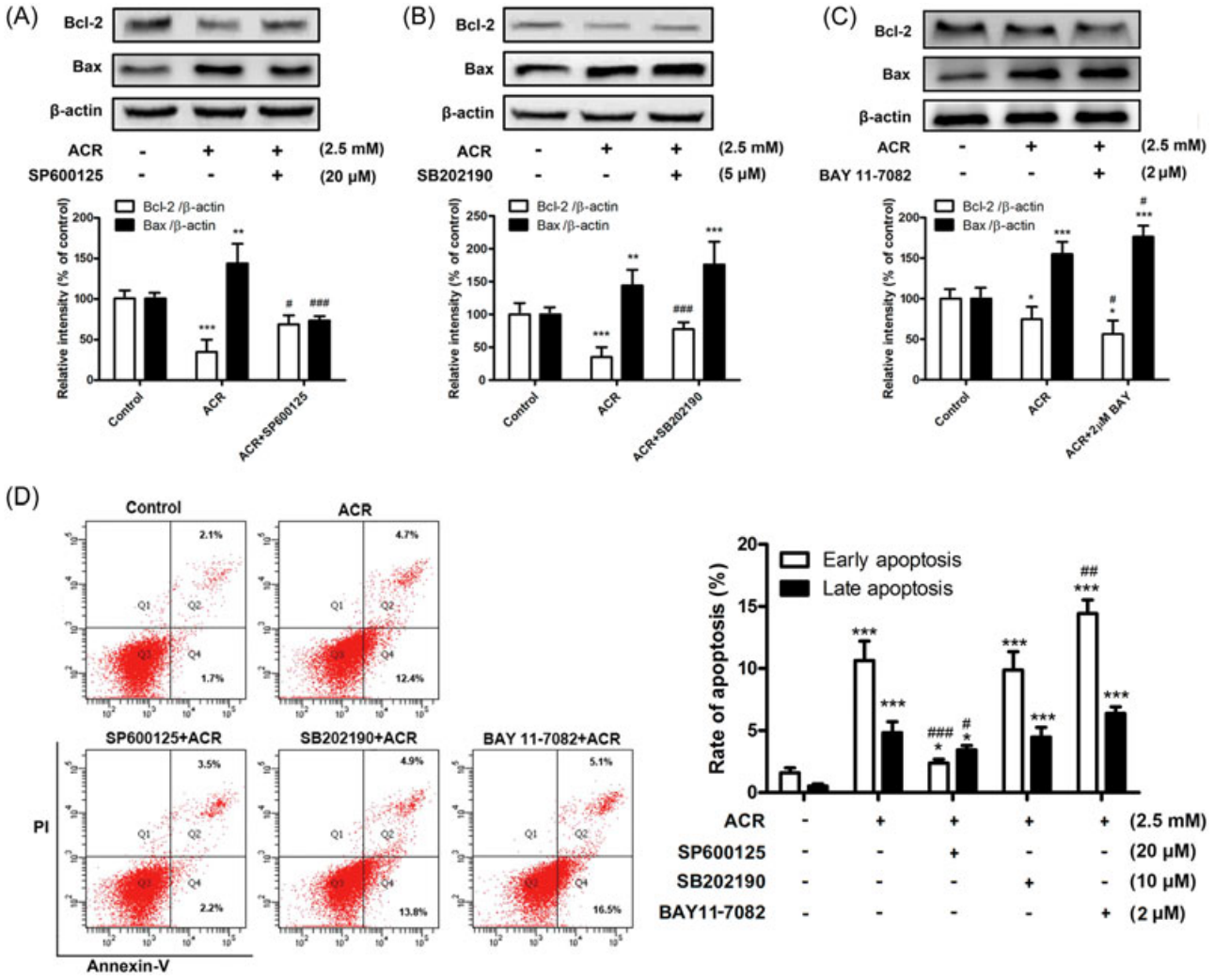

FIGURE 8 Regulatory effects of JNK, p38, and NF-κB on ACR induced the apoptosis of SH-SY5Y cells. Cells were pretreated with SP600125 (20 μM) (A), SB202190 (10 μM) (B), and BAY 11-7082 (2 μM) (C) for 2 hours, and then exposed to 2.5 mM ACR for 24 hours. Protein extract was used to determine the expression levels of Bcl-2 and Bax by Western blot analysis. Statistical analysis of Bcl-2 and Bax expression were performed as fold increases in optical density with β-actin serving as the internal control. The proportions of living and apoptotic cells were detected by flow cytometry analysis using annexin V-FITC/PI test (D). Living cells were unlabeled with annexin V/PI (Q3), whereas early apoptotic cells were labeled with annexin V (Q4). Cells showing annexin and PI double labeling (Q2) represent late apoptosis. Ten thousand cells were analyzed in each sample. The percentages of early apoptotic and late apoptotic cells based on the total cell population analyzed were determined. Data are expressed as mean ± SD ($n = 6$). $^{*}P < 0.05$, $^{**}P < 0.01$, $^{***}P < 0.001$ vs the vehicle controls; $^{\#}P < 0.05$, $^{\#\#}P < 0.01$, $^{\#\#\#}P < 0.001$ vs ACR treatment groups. ACR, acrylamide; Bax, Bcl-2-associated X protein; Bcl-2, B-cell lymphoma 2; FITC, fluorescein isothiocyanate; JNK, c-Jun N-terminal kinase; NF-κB, nuclear factor κB; PI, propidium iodide

studies proposed that oxidative stress is a key factor in ACR-induced neurotoxicity in rats.[14,23] Oxidative stress is due to the imbalance between the systemic production of oxidation products and antioxidant defenses against free radicals. MDA, an indicator of oxidative stress, is used as a diagnostic marker of lipid peroxidation damage. Nonenzymatic antioxidant GSH is vital for alleviating oxidative damage. Our present results showed dose dependently increased MDA and decreased GSH in both rat striatum and SH-SY5Y cells especially that GSH decreased even in low dose of ACR group, suggesting GSH consumption is a sensitive indicator of ACR poisoning. GSH deletion is a key event in ACR-induced oxidative stress, because ACR and its metabolite GA are metabolized and detoxified by GSH, resulting in reduced regeneration of the sulfhydryl group.[24,25] Apart from GSH, ACR could also change the levels of antioxidant enzymes. In our previous publication, ACR caused significant decrease in the activities of SOD and glutathione peroxidase (GSH-Px), which could be alleviated by antioxidant melatonin.[14] Other similar studies have also reported that ACR-induced neurotoxicity was associated with the enhancement of lipid peroxidation and reduction of the antioxidative capacity such as GSH-Px, GSH, SOD, which were remitted by

some antioxidants chemical.[26-29] Nrf2 signaling is another way to restore and maintain cellular oxidative stress at the nontoxic level. Under oxidative stress, Nrf2 quickly dissociates from Keap1, and subsequently translocates into nucleus where it binds to antioxidant response element and ultimately activates the phase II detoxifying enzymes. Nrf2 signaling played an important role in protection against oxidative damage and cell death.[30] However, nuclear Nrf2 was not significantly upregulated in ACR-treated rats, indicating that declined antioxidant defenses led to oxidative stress and the resultant ACR-induced neuropathy in our animal model.

The intercellular oxidative stress status is known to activate NF-κB signaling,[31-33] which regulates a number of genes involved in inflammation and immune responses that typically contribute to cell death and tissue destruction following stressful stimuli.[34] Inflammation of the central nervous system is a prominent feature in many neurodegenerative diseases.[35] In the current study, we found that ACR induced a significant increase in the nuclear NF-κB expression and the release of its downstream target inflammatory cytokines TNF-α and IL-6 both in vivo and in vitro, indicating NF-κB signaling mediated ACR-induced inflammatory response. These results were very similar to a recent study which suggested ACR caused inflammatory response and subsequently amplified the inflammatory response by releasing various cytokines in mice.[33]

MAPKs pathway is reported to be associated with cell proliferation, differentiation, migration, senescence, and apoptosis. Our in vivo data found that ACR exposure caused sustained activation of JNK and p38. It is reported that sustained activation of JNK and p38 usually causes neuronal death.[36-38] Here, we explored the contribution of JNK and p38 pathways to ACR-induced apoptosis in our cell models by inhibiting JNK and p38 pathways, respectively. Suppression of p38 pathway by SB202190 did not change the proportion of apoptotic cells compared with the ACR group. Blockade of JNK by SP600125 upregulated the reduced Bcl-2 expression and downregulated the increased Bax level induced by ACR, thereby eventually attenuated the early and late apoptosis of cells, suggesting the JNK signaling pathway plays an important role in regulating ACR-induced apoptosis. NF-κB activation is a double-edged sword, exhibiting apparently conflicting roles in neuronal apoptosis and survival. NF-κB activation is an essential event in p53-mediate apoptosis and contributory to cell death in cerebral ischemia.[39] On the contrary, there is evidence suggesting that NF-κB activation was responsible for resistance p53-mediated neuronal death, and closely related to neuronal survival and plasticity.[40] One study found that inhibition of NF-κB signaling induced cerebellar granule cell death.[41] In the current work, inhibitory test was conducted to explore the role of NF-κB pathway in ACR-induced apoptosis. The results showed that inhibition of NF-κB activity markedly upregulated the level of Bax and decreased the Bcl-2 expression, eventually resulting in increased proportions of apoptotic cells, which supported the notion that NF-κB is a protective regulator in response to ACR exposure.

The relationship among ROS, NF-κB, and JNK phosphorylation was investigated in PC12 cells in our previous study.[42] We found the ROS scavenger, *N*-acetylcysteine protected against ACR-induced oxidative damage via suppressing NF-κB expression. Blockade of JNK by specific inhibitor SP60015 significantly attenuated ACR-induced accumulation of NF-κB, indicating the activation of NF-κB was mediated through JNK phosphorylation in ACR-treated PC12 cells.

In summary, the roles of MAPKs and NF-κB signaling pathways in ACR-induced neuropathy and apoptosis were studied in vivo and in vitro. Acute exposure to ACR by intracerebroventricular injection caused apoptosis and loss of dopaminergic neurons, elicited oxidative stress and inflammatory response. NF-κB and MAPKs signaling pathways were activated by ACR. JNK contributed to ACR-induced apoptosis, while NF-κB was a protective regulator in response to the apoptosis caused by ACR. The findings added to our understanding of the mechanisms of ACR-induced neurotoxicity.

ACKNOWLEDGMENTS

We appreciate the contribution of all the members participating in this study. The work was financially supported by the National Natural Science Foundation of China (no. 81373042).

CONFLICTS OF INTEREST

The authors declare that there are no conflicts of interest.

ORCID

Dandan Yan http://orcid.org/0000-0001-8421-2593

REFERENCES

1. Mottram DS, Wedzicha BL, Dodson AT. Acrylamide is formed in the Maillard reaction. *Nature*. 2002;419(6906):448-449. https://doi.org/10.1038/419448a
2. Tareke E, Rydberg P, Karlsson P, Eriksson S, Törnqvist M. Analysis of acrylamide, a carcinogen formed in heated foodstuffs. *J Agric Food Chem*. 2002;50(17):4998-5006.
3. Lim TG, Lee BK, Kwon JY, Jung SK, Lee KW. Acrylamide upregulates cyclooxygenase-2 expression through the MEK/ERK

signaling pathway in mouse epidermal cells. *Food Chem Toxicol*. 2011;49(6):1249-1254. https://doi.org/10.1016/j.fct.2011.03.003

4. Lopachin RM, Gavin T. Acrylamide-induced nerve terminal damage: relevance to neurotoxic and neurodegenerative mechanisms. *J Agric Food Chem*. 2008;56(15):5994-6003. https://doi.org/10.1021/jf703745t
5. Erkekoglu P, Baydar T. Acrylamide neurotoxicity. *Nutr Neurosci*. 2014;17(2):49-57. https://doi.org/10.1179/1476830513y.0000000065
6. Lehning EJ, Balaban CD, Ross JF, Reid MA, LoPachin RM. Acrylamide neuropathy. I. Spatiotemporal characteristics of nerve cell damage in rat cerebellum. *Neurotoxicology*. 2002;23(3):397-414.
7. Blackburn JR, Pfaus JG, Phillips AG. Dopamine functions in appetitive and defensive behaviours. *Prog Neurobiol*. 1992;39(3):247-279.
8. Li XM, Xu CL, Deng JM, Li LF, Ma SP, Qu R. Protective effect of Zhen-Wu-Tang (ZWT) through keeping DA stable and VMAT 2/DAT mRNA in balance in rats with striatal lesions induced by MPTP. *J Ethnopharmacol*. 2011;134(3):768-774. https://doi.org/10.1016/j.jep.2011.01.040
9. Pardridge WM. Drug transport in brain via the cerebrospinal fluid. *Fluids Barriers CNS*. 2011;8(1):7. https://doi.org/10.1186/2045-8118-8-7
10. Yao X, Zhang Y, Yan L, et al. Acrylamide exposure impairs blood-cerebrospinal fluid barrier function. *Neural Regen Res*. 2014;9(5):555-560. https://doi.org/10.4103/1673-5374.130080
11. Li D, Wang P, Liu Y, Hu X, Chen F. Metabolism of acrylamide: interindividual and interspecies differences as well as the application as biomarkers. *Curr Drug Metab*. 2016;17(4):317-326.
12. Paulsson B, Kotova N, Grawé J, et al. Induction of micronuclei in mouse and rat by glycidamide, genotoxic metabolite of acrylamide. *Mutat Res*. 2003;535(1):15-24.
13. LoPachin RM, Gavin T. Molecular mechanism of acrylamide neurotoxicity: lessons learned from organic chemistry. *Environ Health Perspect*. 2012;120(12):1650-1657. https://doi.org/10.1289/ehp.1205432
14. Pan X, Zhu L, Lu H, Wang D, Lu Q, Yan H. Melatonin Attenuates oxidative damage induced by acrylamide in vitro and in vivo. *Oxid Med Cell Longev*. 2015;2015. 703709-12. https://doi.org/10.1155/2015/703709
15. Dasuri K, Zhang L, Keller JN. Oxidative stress, neurodegeneration, and the balance of protein degradation and protein synthesis. *Free Radic Biol Med*. 2013;62:170-185. https://doi.org/10.1016/j.freeradbiomed.2012.09.016
16. Wooten MW. Function for NF-kB in neuronal survival: regulation by atypical protein kinase C. *J Neurosci Res*. 1999;58(5):607-611.
17. Yan J, Greer J. NF-kappa B, a potential therapeutic target for the treatment of multiple sclerosis. *CNS Neurol Disord Drug Targets*. 2008;7(6):536-557.
18. Camandola S, Mattson MP. NF-kappa B as a therapeutic target in neurodegenerative diseases. *Exp Opin Ther Targets*. 2007;11(2):123-132. https://doi.org/10.1517/14728222.11.2.123
19. Nguyen T, Nioi P, Pickett CB. The Nrf2-antioxidant response element signaling pathway and its activation by oxidative stress. *J Biol Chem*. 2009;284(20):13291-13295. https://doi.org/10.1074/jbc.R900010200
20. Lee S, Park HR, Lee JY, et al. Learning, memory deficits, and impaired neuronal maturation attributed to acrylamide. *J Toxicol Environ Health A*. 2018;81(9):254-265. https://doi.org/10.1080/15287394.2018.1440184
21. Waisman A, Liblau RS, Becher B. Innate and adaptive immune responses in the CNS. *Lancet Neurol*. 2015;14(9):945-955. https://doi.org/10.1016/s1474-4422(15)00141-6
22. Xu J, Dong H, Qian Q, et al. Astrocyte-derived CCL2 participates in surgery-induced cognitive dysfunction and neuroinflammation via evoking microglia activation. *Behav Brain Res*. 2017;332:145-153. https://doi.org/10.1016/j.bbr.2017.05.066
23. Yousef MI, El-Demerdash FM. Acrylamide-induced oxidative stress and biochemical perturbations in rats. *Toxicology*. 2006;219(1-3):133-141. https://doi.org/10.1016/j.tox.2005.11.008
24. Sumner SCJ, MacNeela JP, Fennell TR. Characterization and quantitation of urinary metabolites of [1,2,3-13C]acrylamide in rats and mice using 13C nuclear magnetic resonance spectroscopy. *Chem Res Toxicol*. 1992;5(1):81-89.
25. Friedman M. Chemistry, biochemistry, and safety of acrylamide. A review. *J Agric Food Chem*. 2003;51(16):4504-4526. https://doi.org/10.1021/jf030204+
26. Li L, Sun H, Liu W, Zhao H, Shao M. Silymarin protects against acrylamide-induced neurotoxicity via Nrf2 signalling in PC12 cells. *Food Chem Toxicol*. 2017;102:93-101. https://doi.org/10.1016/j.fct.2017.01.021
27. Santhanasabapathy R, Vasudevan S, Anupriya K, Pabitha R, Sudhandiran G. Farnesol quells oxidative stress, reactive gliosis and inflammation during acrylamide-induced neurotoxicity: Behavioral and biochemical evidence. *Neuroscience*. 2015;308:212-227. https://doi.org/10.1016/j.neuroscience.2015.08.067
28. Song J, Zhao M, Liu X, Zhu Y, Hu X, Chen F. Protection of cyanidin-3-glucoside against oxidative stress induced by acrylamide in human MDA-MB-231 cells. *Food Chem Toxicol*. 2013;58:306-310. https://doi.org/10.1016/j.fct.2013.05.003
29. Zhu YJ, Zeng T, Zhu YB, et al. Effects of acrylamide on the nervous tissue antioxidant system and sciatic nerve electrophysiology in the rat. *Neurochem Res*. 2008;33(11):2310-2317. https://doi.org/10.1007/s11064-008-9730-9
30. Baird L, Dinkova-Kostova AT. The cytoprotective role of the Keap1-Nrf2 pathway. *Arch Toxicol*. 2011;85(4):241-272. https://doi.org/10.1007/s00204-011-0674-5
31. Morcos M, Schlotterer A, Sayed A, et al. Rosiglitazone reduces angiotensin II and advanced glycation end product-dependent sustained nuclear factor-kappaB activation in cultured human proximal tubular epithelial cells. *Horm Metab Res*. 2008;40(11):752-759. https://doi.org/10.1055/s-0028-1082039
32. Sayed AAR. Thymoquinone protects renal tubular cells against tubular injury. *Cell Biochem Funct*. 2008;26(3):374-380. https://doi.org/10.1002/cbf.1454
33. Zhang L, Wang E, Chen F, Yan H, Yuan Y. Potential protective effects of oral administration of allicin on acrylamide-induced toxicity in male mice. *Food Funct*. 2013;4(8):1229-1236. https://doi.org/10.1039/c3fo60057b
34. Baeuerle PA, Henkel T. Function and activation of NF-kappa B in the immune system. *Annu Rev Immunol*. 1994;12:141-179. https://doi.org/10.1146/annurev.iy.12.040194.001041

35. Lim M. Treating inflammation in childhood neurodegenerative disorders. *Dev Med Child Neurol*. 2011;53(4):298-304. https://doi.org/10.1111/j.1469-8749.2010.03902.x
36. Park SE, Sapkota K, Choi JH, et al. Rutin from Dendropanax morbifera Leveille protects human dopaminergic cells against rotenone induced cell injury through inhibiting JNK and p38 MAPK signaling. *Neurochem Res*. 2014;39(4):707-718. https://doi.org/10.1007/s11064-014-1259-5
37. Sproul AA, Xu Z, Wilhelm M, Gire S, Greene LA. Cbl negatively regulates JNK activation and cell death. *Cell Res*. 2009;19(8):950-961. https://doi.org/10.1038/cr.2009.74
38. Hetman M, Xia Z. Signaling pathways mediating anti-apoptotic action of neurotrophins. *Acta Neurobiol Exp (Wars)*. 2000;60(4):531-545.
39. Zhang W, Potrovita I, Tarabin V, et al. Neuronal activation of NF-kappaB contributes to cell death in cerebral ischemia. *J Cereb Blood Flow Metab*. 2005;25(1):30-40. https://doi.org/10.1038/sj.jcbfm.9600004
40. Culmsee C, Siewe J, Junker V, et al. Reciprocal inhibition of p53 and nuclear factor-kappaB transcriptional activities determines cell survival or death in neurons. *J Neurosci*. 2003;23(24):8586-8595.
41. Piccioli P, Porcile C, Stanzione S, et al. Inhibition of nuclear factor-kappaB activation induces apoptosis in cerebellar granule cells. *J Neurosci Res*. 2001;66(6):1064-1073. https://doi.org/10.1002/jnr.1251
42. Pan X, Wu X, Yan D, Peng C, Rao C, Yan H. Acrylamide-induced oxidative stress and inflammatory response are alleviated by N-acetylcysteine in PC12 cells: Involvement of the crosstalk between Nrf2 and NF-kappaB pathways regulated by MAPKs. *Toxicol Lett*. 2018;288:55-64. https://doi.org/10.1016/j.toxlet.2018.02.002

How to cite this article: Yan D, Pan X, Yao J, et al. MAPKs and NF-κB-mediated acrylamide-induced neuropathy in rat striatum and human neuroblastoma cells SY5Y. *J Cell Biochem*. 2018; 1-13. https://doi.org/10.1002/jcb.27671